Original Article

NAD-dependent methylenetetrahydrofolate dehydrogenase inhibits oral squamous cell carcinoma cell proliferation and promotes apoptosis

Liang Zhao[1#], Zhe Cheng[2,3#], Zhiyue Lu[2,3], Jianqiu Jin[2,3]

[1]Department of Stomatology, Aviation General Hospital, China Medical University, Beijing, China; [2]Department of Stomatology, Beijing Hospital, National Center of Gerontology, Beijing, China; [3]Institute of Geriatric Medicine, Chinese Academy of Medical Sciences, Beijing, China

Contributions: (I) Conception and design: L Zhao; (II) Administrative support: J Jin; (III) Provision of study materials or patients: J Jin, Z Cheng; (IV) Collection and assembly of data: Z Lu, Z Cheng; (V) Data analysis and interpretation: L zhao, Z Cheng; (VI) Manuscript writing: All authors; (VII) Final approval of manuscript: All authors

[#]These authors contributed equally to this work.

Correspondence to: Dr. Jianqiu Jin. Department of Stomatology, Beijing Hospital, National Center of Gerontology, Beijing 100730, China; Institute of Geriatric Medicine, Chinese Academy of Medical Sciences, Beijing 100730, China. Email: dentalstudy@126.com.

Background: NAD-dependent methylenetetrahydrofolate dehydrogenase catalyzes the conversion of 10-formyltetrahydrofolate to formate in embryonic and adult mammalian mitochondria. Methylenetetrahydrofolate dehydrogenase 1-like (MTHFD1L) is a folate cycle enzyme that is involved in the development of various diseases including cancer. However, the specific mechanisms in oral squamous cell carcinoma (OSCC) are unclear. We analyzed the functional routes of MTHFD1L in OSCC cells.

Methods: MTHFD1L expression in OSCC was analyzed using data from The Cancer Genome Atlas (TCGA) database. Then, the levels of mRNA were measured in OSCC and para-tumor oral tissues using Affymetrix microarrays. Additionally, the effects of short hairpin RNA (shRNA)-induced MTHFD1L silencing on the biological behavior of OSCC were assessed *in vitro* and *in vivo*, and the potential molecular mechanisms underlying MTHFD1L activity were also investigated.

Results: A TCGA database analysis of RNA sequencing revealed that MTHFD1L levels were higher in tumor tissue than in adjacent tissues. Immunohistochemical staining and Kaplan-Meier survival analysis also indicated that MTHFD1L upregulation is associated with a poor prognosis in OSCC. The knockdown of MTHFD1L suppressed cell proliferation, colony formation, and tumorigenesis, while it induced apoptosis in OSCC. Mechanistically, a microarray analysis showed that MTHFD1L suppressed c-MYC and activated p53 signaling by regulating the protein expression of *TP53*, *GADD45A*, *FAS* and *JUN*.

Conclusions: MTHFD1L may be involved in OSCC progression via the *c-MYC* gene and p53 signaling and may serve as a novel target and orientation for tumor therapy.

Keywords: Methylenetetrahydrofolate dehydrogenase 1-like (MTHFD1L); oral squamous cell carcinoma (OSCC); proliferation; c-MYC; p53 signaling pathway

Submitted Aug 27, 2020. Accepted for publication Jan 08, 2020.
doi: 10.21037/tcr-20-2798
View this article at: http://dx.doi.org/10.21037/tcr-20-2798

Introduction

Many recent studies have focused on the role of folic acid, especially its relationship with the risk of cancer. These studies discuss the relationship between folic acid and various solid tumors (1,2). The incidence and mortality of cancer in patients receiving folic acid and VB12 were explored in two double-blind, randomized, controlled clinical trials in Norway. Surprisingly, folate therapy was

associated with increased cancer incidence, cancer mortality, and all-cause mortality (3). Low levels of folic acid can lead to DNA replication, methylation and repair dysfunction. Moreover, researchers assessed the relationship between folate intake and risks of head and neck cancer (HNC) using prospective data from prostate, lung, colorectal cancer, and ovarian cancer. One particular study included 186 cases with a confirmed incidence of HNC. Using a Cox proportional hazard model, the authors found that higher dietary folate intake and enhanced folate intake were dose-related to HNC risk reduction (4).

Folic acid is an essential nutrient with a biological function that provides methylation materials for intracellular DNA methylation and thymidine synthesis. Folate metabolism disorders may disrupt methylation and affect DNA synthesis and repair, which can lead to cancer (5). The human gene for methylenetetrahydrofolate dehydrogenase ($NADP^+$ dependent) 1-like (MTHFD1L) encodes monofunctional C1-tetrahydrofolate synthase, which is a mitochondrial protein with monofunctional 10-formyl-tetrahydrofolate synthetase activity (6,7). As a component of folate-mediated one-carbon metabolism, human mitochondrial monofunctional 10-formyl-tetrahydrofolate synthetase is tightly associated with the matrix side of the mitochondrial inner membrane and catalyzes the conversion of 10-formyl-tetrahydrofolate to formate in both embryonic and adult mammalian mitochondria. Then, formate is transported from the mitochondria to the cytoplasm, where it is involved in the cytoplasmic branch of folate-dependent one-carbon metabolism, and this makes it indispensable in cytoplasmic processes such as purine biosynthesis, thymidylate biosynthesis, and the methyl cycle (8).

MTHFD1L is critical for cell growth, which is associated with multiple malignant tumors (9-11). Li *et al*. investigated the roles of MTHFD1L silencing in cell proliferation and apoptosis in tongue squamous cell carcinoma (TSCC) but its exact mechanism remains unclear (9). Carcinogenesis is a multifactorial phenomenon involving numerous genetic and epigenetic events and can alter the function of tumor suppressor genes, oncogenes, and other related molecules (12). Concurrently, OSCC is a highly complex multistep process involving the progressive acquisition of genetic and epigenetic alterations and dynamic genomic changes. Current methods of molecular testing remain deficient in their effect on treatment selection for oral cancer (13). Therefore, the identification of suitable biomarkers for early diagnosis and treatment is urgently required in OSCC. We present the following article in accordance with the MDAR checklist (available at http://dx.doi.org/10.21037/tcr-20-2798).

Methods

Bioinformatic analysis

Data from head and neck squamous cell carcinoma (HNSCC) patients from TCGA (TCGA public data; November 2, 2017, http://tcga-data.nci.nih.gov/) were analyzed. In total, 528 samples were available in the TCGA database, including 520 RNAseqV2 samples and 40 pairs of samples with pathological data and HNSCC tumor tissue with corresponding adjacent normal tissues. This expression profile was based on RNAseqV2 data from 40 paired samples. Gene expression data were normalized to RNA normalization using the Trimmed Mean of M-values (TMM) method. To prevent incorrect sample-grouping errors, a quality control procedure was performed based on of the biological coefficient of variation (BCV).

Immunohistochemical (IHC) staining and survival analysis

Tumor and matched para-tumor tissues were acquired from 96 OSCC patients who were histologically diagnosed at Beijing Hospital. The tissue samples were immediately frozen in liquid nitrogen after removal and stored at −80 ℃ until ready for use. The study was conducted in accordance with the Declaration of Helsinki (as revised in 2013). The study was approved by ethics board of Beijing Hospital (BJ200768X2). Written informed consent form was obtained from all patients. Surgical specimens of OSCC were obtained from June 2007 to July 2016, and 96 patients were involved in a follow-up cohort study until August 2017.

The tissue sections were deparaffinized and blocked in 0.03% hydrogen peroxidase. After heating in a microwave for 10 min and cooling to room temperature, the sections were incubated with blocking serum (10% Tris-buffered saline) for 30 min and incubated with rabbit anti-human MTHFD1L antibody (1:200, SIGMA, Cat. No. HPA029040, San Francisco, USA) at 4 ℃ overnight. IHC staining was blindly evaluated by two pathologists.

Cell lines and cell culture

OSCC cell lines CAL-27 and SCC-25 and the human

embryonic kidney cell line 293 were purchased from the Cell Resource Centre, Shanghai Institute for Biological Sciences, Chinese Academy of Science. Cells were cultured in Dulbecco's Modified Eagle's Medium (DMEM) (Corning, NY, USA) that was supplemented with 10% fetal calf serum (Cat. # A11-102, Ausbian) at 37 ℃ with 5% CO_2 in a humidified atmosphere. The cell lines were tested and authenticated on Oct 20th, 2017, via short tandem repeat (STR) analysis.

MTHFD1L short hairpin RNA (shRNA) design and lentivirus construction

To repress MTHFD1L expression, a shRNA fragment specifically targeting MTHFD1L was designed (GeneChem, Shanghai, China). The lentiviral vectors expressing MTHFD1L shRNA were constructed, and the knockdown efficiency was confirmed Briefly, shRNA with a target sequence of 5'-ATTCCAGTTCCTGTATGAT-3' targeting MTHFD1L was designed, and a scrambled shRNA with sequence 5'-TTCTCCGAACGTGTCACGT-3' was used as the negative control (NC). Related stem-loop DNA oligonucleotides were synthesized, annealed, and inserted into the GV115 PSCSI-GFP lentiviral vector at AgeI/EcoRI sites. The final lentiviral plasmid constructs were co-transfected into 293 cells to generate lentiviruses. For the lentivirus infection, cells were seeded into six-well plates and cultured until the cell monolayers were 70% confluent. The lentiviruses were then added to the cells at a multiplicity of infection (MOI) of 20. After 72 h, the cells were examined using a fluorescence microscope and harvested for subsequent experiments. The knockdown efficiency was evaluated using reverse transcription-quantitative polymerase chain reaction (RT-qPCR) and Western blot.

RNA extraction and RT-qPCR analysis

The total cellular RNA was isolated from cultured cells using TRIzol reagent (Cat. #3101-100, Shanghai Pufei Biotechnology Co. Ltd., Nanjing, China). RNA was quantified using a Nanodrop 2000 spectrophotometer (Thermo Fisher Scientific) and reverse transcription of 2 μg of RNA and using the Moloney Murine Leukemia Virus (M-MLV) reverse transcription kit in accordance with the manufacturer's instructions. qPCR was conducted using the two-step method and following the manufacturer's procedure. The procedure utilized the following amplification: hold at 95 ℃ for 30 seconds for pre-denaturation; 40 cycles of 5 s at 95 ℃ for denaturation and 30 s at 60 ℃ for elongation. Primers were purchased from Ribobio (Guangzhou, China). The primers for RT-qPCR included a MTHFD1L forward primer (5'-TCACTCACATTTGCCTCCCTC-3') and a reverse primer (5'-CTGAAGGGCAAGGCCATGTA-3') as well as GAPDH forward primer (5'-TGACTTCA ACAGCGACACCCA-3') and a reverse primer (5'-C ACCCTGTTGCTGTAGCCAAA-3'). GAPDH was used as an internal control. The $2^{-\Delta\Delta Ct}$ method was used to quantitatively analyze the relative changes in gene expression.

Western blot assay

For the whole-cell protein extraction, cells were harvested and lysed on ice for 15 min in a lysis buffer containing 100 mM Tris-HCl, 2% mercaptoethanol, 20% glycerin, and 4% sodium dodecyl sulfate (SDS). The protein concentration in the clarified lysates was determined using a BCA protein assay kit (Ding Guo Biotechnology, Beijing, China) using the manufacturer's instructions. Equal amounts of proteins were separated using SDS-polyacrylamide gel electrophoresis (SDS-PAGE) and then transferred to polyvinylidene difluoride (PVDF) membranes (Millipore). Membranes were blocked for 1 h at room temperature with 5% fat-free milk in Tris-buffered saline and Tween-20 (TBST) buffer. Then, membranes were incubated with primary antibodies, including anti-MTHFD1L (1:200, Sigma-Aldrich Cat# HPA029040, RRID:AB_2672879), anti-TP53 (1:300, Atlas Antibodies Cat# HPA051244, RRID:AB_2681403), anti-JUN (1:200, Atlas Antibodies Cat# HPA059474, RRID:AB_2684030), anti-GADD45A (1:200, Atlas Antibodies Cat#HPA053420, RRID:AB_2682144), anti-FAS (1:300, Atlas Antibodies Cat#HPA027444, RRID:AB_10601378), anti-MYC (1:100, Santa Cruz Biotechnology Cat#sc-789, RRID:AB_631274), or anti-GAPDH (1:2,000, Atlas Antibodies Cat#HPA040067, RRID:AB_10965903), overnight at 4 ℃. After incubation, membranes were washed in TBST and incubated with the corresponding horseradish peroxidase (HRP)-conjugated secondary antibody (1:2,000) for 1.5 h at room temperature. Then, membranes were washed and developed in TBST buffer. The immunoreactive bands were visualized using a chemiluminescent Pierce™ ECL Western Blotting Substrate Kit (Thermo Fisher Scientific) with subsequent exposure to X-ray film (Cat. #038401501, Carestream).

Cell proliferation assays

After infection with lentiviruses expressing sh-MTHFD1L or scrambled shRNA, OSCC cells were cultured for 48 h and harvested during the logarithmic phase. Next, cell suspensions were generated and seeded in triplicate in 96-well plates at a density of 1,000 cells per well. After culturing at 37 ℃ with 5% CO_2 for an additional 24 h, images of the cell were captured daily for 5 d using a Celigo image cytometer system (Nexcelom; Lawrence, MA, USA). Cell numbers per well were also quantified using the Celigo system, and cell growth curves were plotted for each condition.

The cell viability was assessed using the MTT (Genview, Beijing, China) assay. Briefly, 1,500 shRNA-treated or untreated cells per well were seeded in 96-well plates. After 24 h at 37 ℃, MTT (5 mg/mL) was added to each well before the terminal point of cell culture, and cells were incubated for an additional 4 h. Then, the medium was removed and formazan crystals were dissolved in 100 μL dimethyl sulfoxide (DMSO). The cell viability was determined by measuring the absorbance of each well at 490/570 nm and using a multi-well plate reader (Cat. #M2009PR; Tecan Infinite).

Colony formation assay

After infection with lentivirus expressing sh-MTHFD1L or scrambled shRNA, OSCC cells were enumerated and plated at a density of 800 cells per well into six-well plates in triplicate. After incubation in a 5% CO_2 incubator at 37 ℃ for 14 d, cells were washed with phosphate-buffered saline (PBS) and fixed with 4% paraformaldehyde (Sinopharm Chemical Reagent, Shanghai, China) for 30–60 min. Then, colonies were stained with Giemsa (Shanghai DingGuo Biotech, Shanghai, China) for 20 min, and images of cell plates were captured using a digital camera and colonies were enumerated for each treatment group.

Cell apoptosis analysis

An annexin-V-APC apoptosis detection kit (eBioscience, Cat. No. 88-8007, San Diego, CA, USA) was used to detect apoptosis using the manufacturer's instructions. Prepared cells were harvested, washed with PBS, and suspended at a final density of 1×10^6–1×10^7 cells/mL. Then, 10 μL annexin-V-APC was mixed with 200 μL of the cell suspension and incubated at room temperature in the dark for 10–15 min. Cells were analyzed using a Guava easyCyte HT flow cytometer (Millipore, Darmstadt, Germany), and data were analyzed using Guava InCyte software.

In vivo xenograft tumor assay

Experiments were performed under a project license (LA2019103) granted by ethics board of Peking University, in compliance with institutional guidelines for the care and use of animals. Four-week-old female BALB/c nude mice were obtained from the Shanghai Laboratory Animal Centre. CAL-27 cells were stably transduced with lentivirus vectors harboring the NC (scrambled shRNA) or MTHFD1L-shRNA, which were suspended in PBS (Invitrogen, Waltham, MA, USA). The cells (5×10^6) were subcutaneously injected into the right axilla. Tumor sizes were initially assessed using a caliper, and the body weight was measured 8 d post-grafting. The tumor volume was calculated using the formula V = π/(6× length × width × width). At 27 d, mice were euthanized and the tumors were excised.

DNA microarrays and ingenuity pathway analysis (IPA)

Total RNA from OSCC cells infected with lentivirus expressing either scrambled shRNA (n=3) or MTHFD1L-shRNA (n=3) was extracted using TRIzol reagent. The RNA quantity and quality were assessed using a NanoDrop 2000 spectrophotometer (Thermo Fisher Scientific) and Agilent 2100 bioanalyzer. The Affymetrix GeneChip PrimeView Human Gene Expression Array was used for microarray processing to determine gene expression profiling in accordance with the manufacturer's instructions. Significantly and differentially expressed genes in OSCC were selected based on the following criteria: false discovery rate (FDR) <0.05 and FCAbsolute >1.5 based on volcano plots. Pathway enrichment analysis was performed for all significantly and differentially expressed genes using IPA.

Statistical analysis

Data are presented as the mean ± standard deviation (SD) deviation and three independent experiments were performed. All statistical analyses were conducted using SPSS 18.0 software (SPSS, Inc., Chicago, IL, USA). The differences between two groups were evaluated using a Student's *t*-test or one-way analysis of variance. All

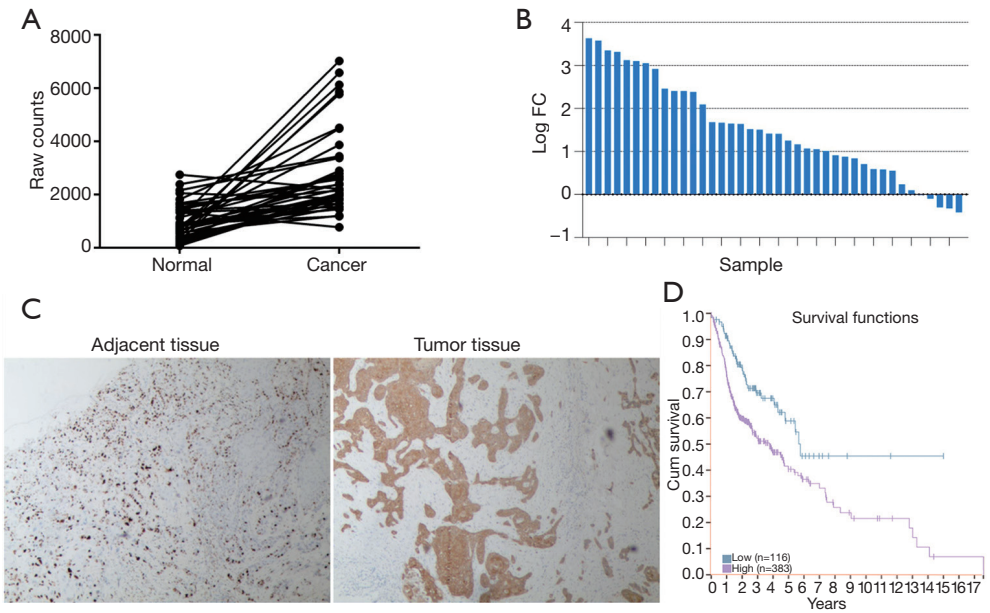

Figure 1 Analysis of MTHFD1L expression based on The Cancer Genome Atlas (TCGA) database. (A) A line chart of the paired comparison of MTHFD1L expression in head and neck squamous cell carcinoma (HNSCC) tumors and adjacent normal tissues. (B) A bar chart of MTHFD1L differential expression in 40 paired samples of tumors and adjacent normal tissues. (C) Representative figures of immunohistochemical staining for MTHFD1L in OSCC tissues and paired adjacent normal tissue (magnification, ×100). (D) A Kaplan-Meier survival curve shows a correlation of overall survival with high and low expression of MTHFD1L in HNSCC. OSCC, oral squamous cell carcinoma.

statistical analyses were two-sided and P values <0.05 were considered statistically significant unless stated otherwise.

Results

Identification of MTHFD1L as a potential gene related to OSCC

We compared the MTHFD1L level in 40 HNSCC tumor specimens registered in the TCGA database with those in the corresponding paired non-tumor adjacent tissues from the same individuals. The TMTHFD1L level was significantly higher in HNSCC than in the adjacent tissue (P<0.05; *Figure 1A*,*B*). We obtained information regarding adjacent tissue and tumor tissue to evaluate MTHFD1L expression using IHC staining in oral specimens in accordance with TCGA. The expression level of MTHFD1L in OSCC tissues from 96 patients was also significantly higher than that in normal tissues (*Figure 1C*). The correlations between MTHFD1L and clinicopathological variables of OSCC are summarized in *Table 1*. MTHFD1L levels correlated with T classification (P=0.002) and local recurrence (P<0.001) in patients with OSCC. No significant difference was observed between the MTHFD1L expression level and any other clinicopathological factor.

Furthermore, a Kaplan-Meier analysis was performed to determine whether MTHFD1L expression was clinically and significantly associated with overall survival in HNSCC patients. To review the TCGA dataset, the mRNA level of MTHFD1L in HNSCC tissues was used as the cut-off point to categorize all cases into MTHFD1L-high (n=116) and -low (n=383) groups. An IPA analysis revealed that the overall survival rates were higher in MTHFD1L-low groups than in MTHFD1L-high groups (*Figure 1D*).

Confirmation of the lentivirus transfection by Western blot and qRT-PCR

A lentivirus-based shRNA strategy was used to knockdown MTHFD1L in human OSCC cell lines. CAL-27 and SCC-25 cells were infected with lentivirus vectors expressing MTHFD1L-shRNA (the knockdown) or scrambled-shRNA (the control). Western blot and qRT-PCR were

Table 1 Correlation between MTHFD1L expression and the clinicopathological characteristics

Characteristic	No. of patients	MTHFD1L		P value
		Low expression, n (%)	High expression, n (%)	
Gender				0.314
Male	44	19 (19.79)	25 (26.04)	
Female	52	28 (29.17)	24 (25.00)	
Age (years)				0.540
≤60	49	22 (22.92)	27 (28.13)	
≥60	47	25 (26.04)	22 (22.92)	
Clinical stage				0.011
I + II	43	29 (30.21)	14 (14.58)	
III + IV	53	18 (18.75)	35 (36.46)	
T classification				0.002
T_1	10	7 (7.29)	3 (3.13)	
T_2	34	24 (25.00)	10 (10.42)	
T_3	45	14 (14.58)	31 (32.29)	
T_4	7	2 (2.08)	5 (5.21)	
N classification				0.011
Yes	26	7 (7.29)	19 (19.79)	
No	70	40 (41.67)	30 (31.25)	
M classification				0.018
Yes	47	10 (10.42)	37 (38.54)	
No	49	22 (22.92)	27 (28.13)	
Local recurrence				<0.001
Yes	65	29 (30.21)	36 (37.50)	
No	31	18 (18.75)	13 (13.54)	

performed to determine the MTHFD1L expression at both mRNA and protein levels. MTHFD1L mRNA levels were reduced by 95.1% in CAL-27 cells and 80.6% for SCC-25 cells compared to the corresponding controls (*Figure 2A*). Accordingly, protein levels were distinctly reduced in the sh-MTHFD1L group compared to the sh-Ctrl group (*Figure 2B*).

MTHFD1L silencing reduces proliferation and clonogenicity of human OSCC cells

We investigated the knockdown effect of MTHFD1L on the cell proliferation of CAL-27 and SCC-25 cells. First, a Celigo cell counting assay was performed to monitor cell proliferation daily for five consecutive days. The number of cells in the sh-Ctrl group temporally increased, whereas only a slight increase in cell number was observed in the sh-MTHFD1L group. A significant difference in cell numbers between the sh-Ctrl and sh-MTHFD1L groups was observed at 5 d post-infection ($P<0.01$). An obvious impairment of cell proliferation was observed at 2 d post-infection in sh-MTHFD1L groups ($P<0.05$; *Figure 3A*). The MTT assay was performed to evaluate the cell proliferation of both cells. Cell proliferation was also significantly inhibited at 5 d post-infection for the sh-MTHFD1L group compared to the sh-Ctrl group ($P<0.01$; *Figure 3B*).

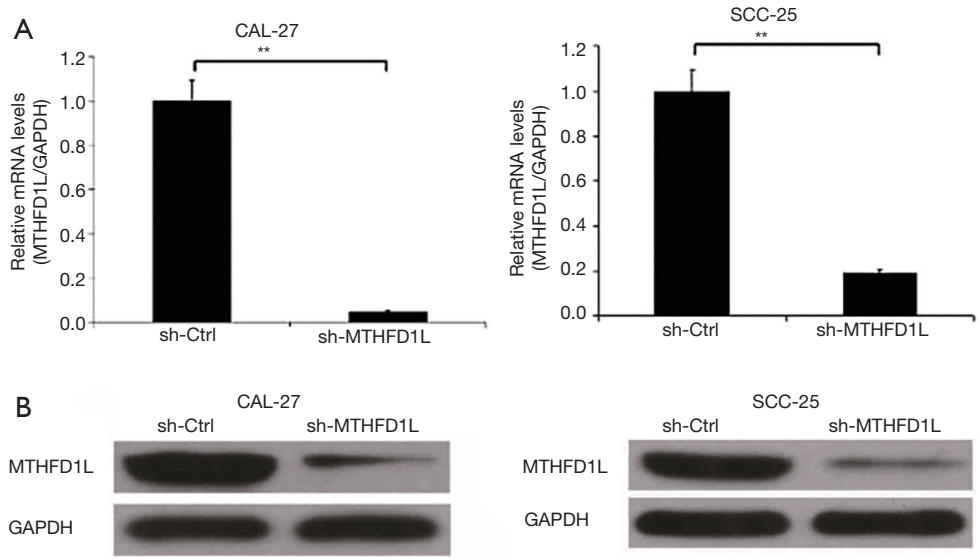

Figure 2 Analysis of MTHFD1L expression via quantitative reverse transcription polymerase chain reaction (RT-qPCR) and Western blot analyses after knockdown. (A) The mRNA expression of MTHFD1L using qRT-PCR in CAL-27 and SCC-25 cells. **, P<0.01. (B) MTHFD1L protein levels in CAL-27 and SCC-25 cells as assessed using Western blot analysis.

Moreover, colony formation analysis results showed that cells treated with sh-MTHFD1L had less clonogenic ability than cells treated with sh-Ctrl (*Figure 3C*).

MTHFD1L silencing induces apoptosis of human OSCC cells

Compared to the sh-Ctrl group, the MTHFD1L knockdown group significantly increased the rate of cell apoptosis in CAL-27 and SCC-25 cells (P<0.01; *Figure 4*). Therefore, MTHFD1L may play an important anti-apoptotic role in OSCC cells.

Silencing of MTHFD1L inhibits tumorigenicity in vivo

Furthermore, to determine whether MTHFD1L promoted OSCC cell tumorigenesis, a xenograft model with stably transfected CAL-27 cells was used in BALB/c nude mice. At 27 d post-grafting, the volumes of MTHFD1L-deficient xenograft tumors were significantly less than those of the NC group (*Figure 5A,B*). After sacrifice, the average tumor weight of the NC group was significantly heavier than that in the MTHFD1L knockdown group (*Figure 5C*). Together, these results indicate that MTHFD1L knockdown effectively reduced the growth of OSCC cells *in vivo*.

Correlation between MTHFD1L expression and the p53 signaling pathway activation level

In total, 673 genes were differentially expressed in OSCC cells expressing sh-MTHFD1L compared to sh-Ctrl cells. Of the differentially regulated genes, 259 were upregulated and 414 were downregulated (*Figure 6A*). Following pathway enrichment analysis, some fundamental biological signaling pathways, such as the p53 and IL-8 signaling pathway, were potentially activated (Z-score ≥2).

To further investigate the related regulatory network of the MTHFD1L-induced malignancy, we analyzed the knowledge-based interactome and constructed a network map of MTHFD1L using IPA. Several genes reportedly involved in tumorigenesis were differentially regulated by MTHFD1L such as *c-MYC*, *TP53*, *GADD45A*, the Fas cell surface death receptor (*FAS*), and *JUN* (*Figure 6B*). These genes were further confirmed via Western blot analysis, which showed that c-MYC and p53-associated proteins TP53, GADD45A, FAS and JUN levels showed a certain degree of difference in MTHFD1L-silenced cells compared with those in control cells (*Figure 6C*). Therefore, these results indicate that MTHFD1L might act as a key regulator of OSCC progression via the c-MYC gene and the p53-dependent pathway.

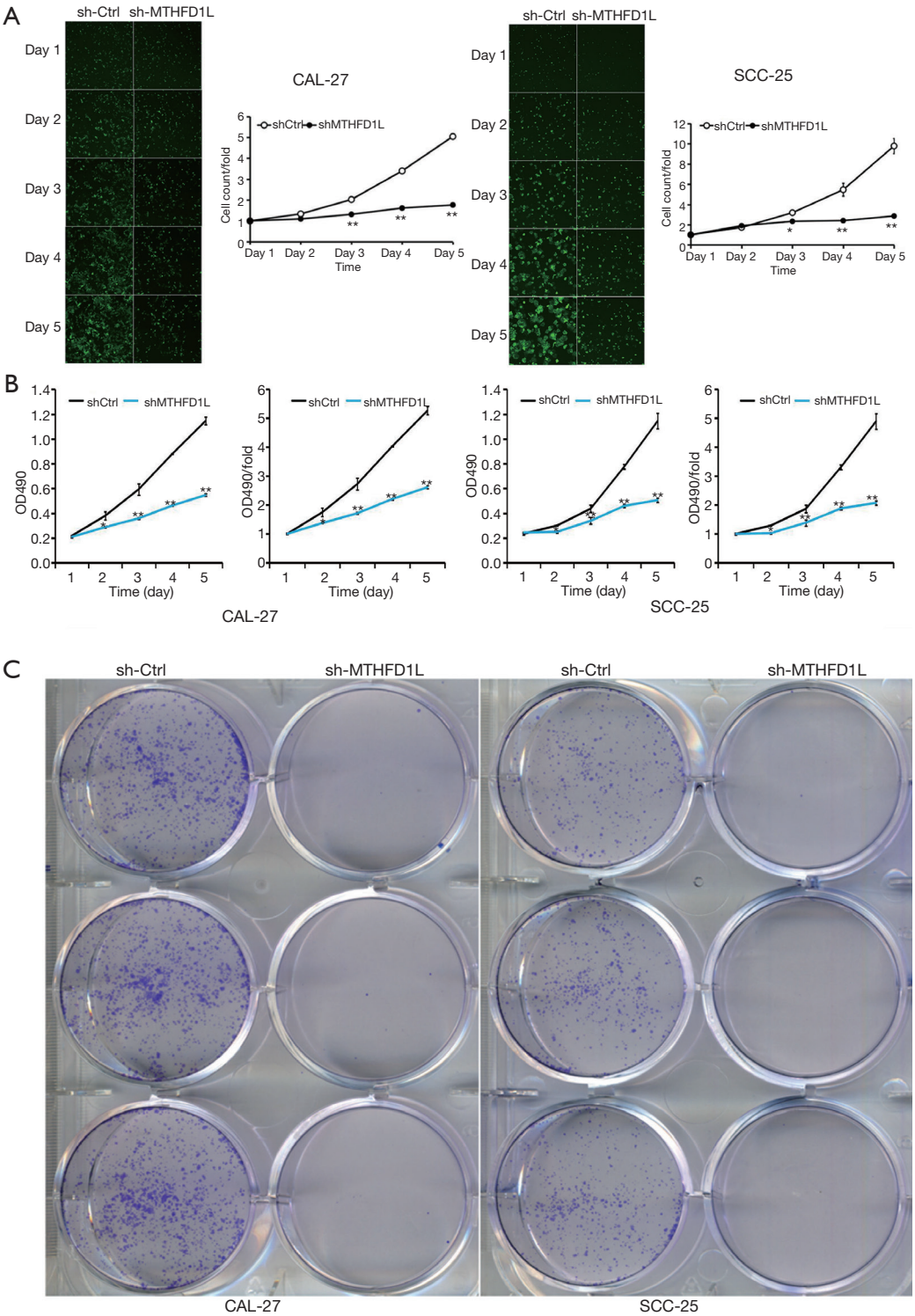

Figure 3 MTHFD1L knockdown inhibits cell growth and proliferation of CAL-27 and SCC-25 cells. (A) Celigo analysis was used to determine the cell proliferation of CAL-27 and SCC-25 through the treatment of sh-MTHFD1L (magnification, ×10). (B) Post-infection cell proliferation determined daily using MTT assays for 5 days. (C) Photographs of Giemsa-stained MTHFD1L colonies in 6-well plates (n=3). The data were obtained independently in triplicate and presented as the mean ± SD. *, P<0.05; **, P<0.01.

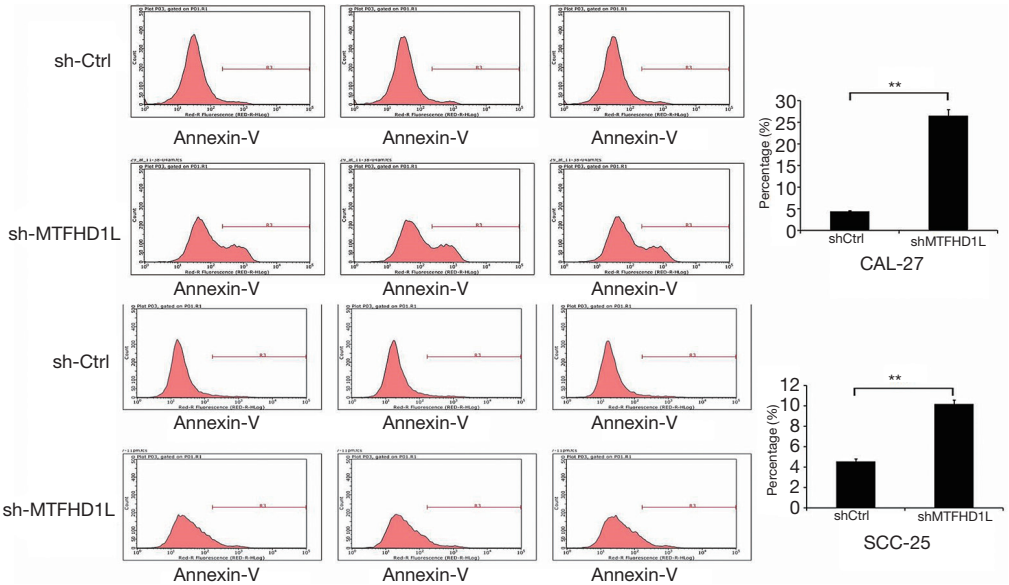

Figure 4 MTHFD1L knockdown increased CAL27 and SCC-25 cell apoptosis. Graphs showing apoptosis in each sample were determined by annexin-V staining, **, P<0.01.

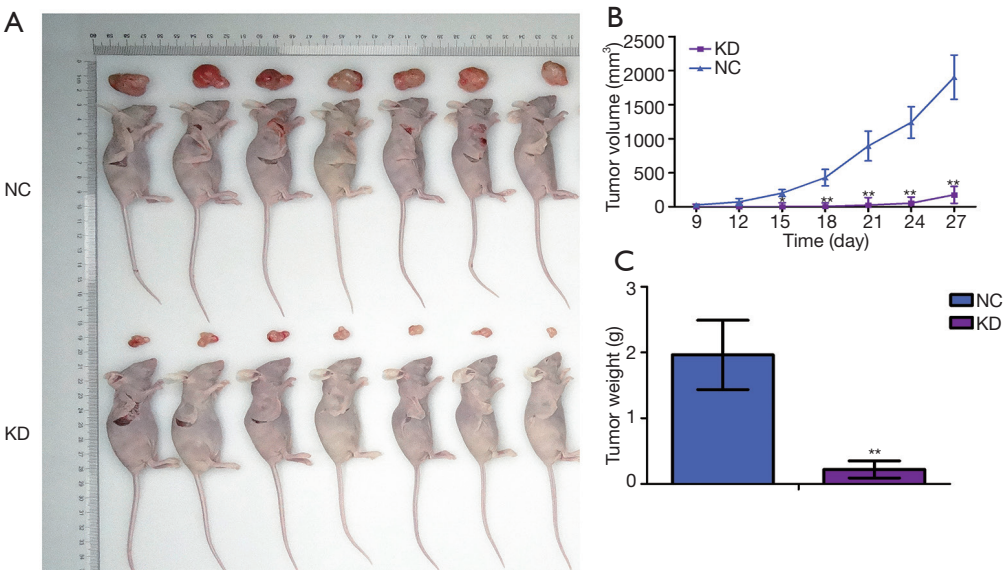

Figure 5 MTHFD1L knockdown in CAL-27 cells suppressed tumor growth in vivo. (A) Xenograft tumors were generated in nude mice (n=7). (B) Tumor size was measured at 9, 12, 15, 18, 21, 24 and 27 d post-grafting seven times; (C) Tumor weight was obtained at 27 d and displayed as the mean ± SD. *, P<0.05; **, P<0.01. NC, negative control; KD, knockdown; SD, standard deviation.

Discussion

A possible relationship between MTHFD1L expression and clinicopathological indices in HNSCC was determined through exploration of the TCGA database. Furthermore, MTHFD1L expression in tumor tissue and normal tissues was reviewed using data from the Human Protein Atlas (HPA). IHC revealed that MTHFD1L expression is higher in tumor tissue than in normal tissues. More importantly, a Kaplan-Meier analysis was also performed to determine

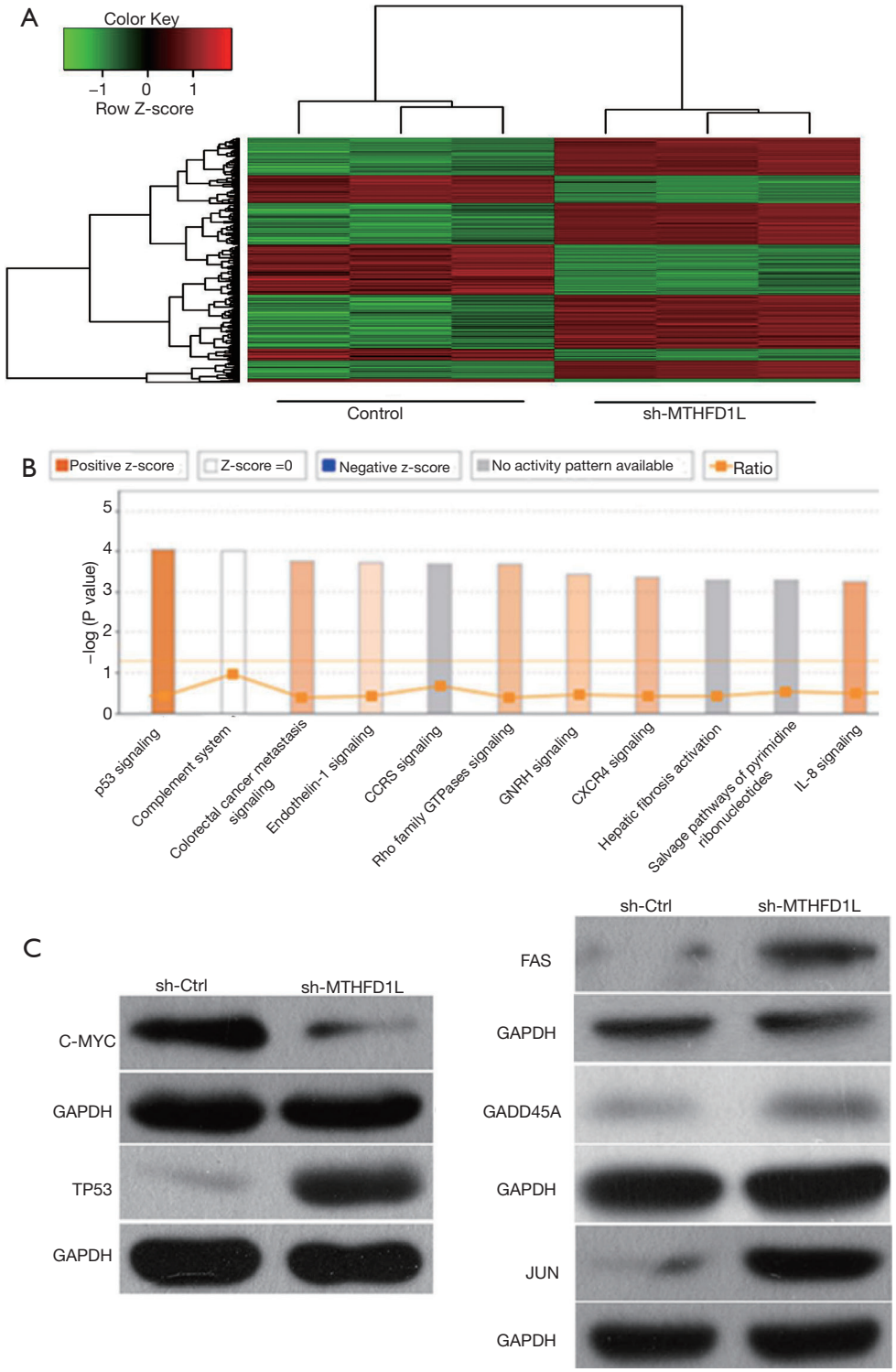

Figure 6 Gene expression profiling identified an association between changes in MTHFD1L expression. (A) Hierarchical clustering of differentially expressed transcripts. The red dots represent upregulated relative expression, whereas green dots indicate relative downregulation. (B) Classical Pathway analysis identified genes enriched after MTHFD1L knockdown. Orange marks indicate activated (Z-score >0) and blue marks indicate suppressed pathways (Z-score <0). (C) Confirmation of the microarray results using Western blot analysis of c-MYC, TP53, GADD45A, FAS and JUN in tumor tissue. GAPDH was used as the internal control.

whether MTHFD1L expression was clinically and significantly associated with overall survival in HNSCC patients. The results indicate that the *MTHFD1L* gene was highly expressed and related to survival.

Cells that preferentially utilize glucose and glutamine to supply and maintain cell mitosis were grown (14). It is clear that metabolites of the folic acid cycle, such as methionine, antioxidant NADPH and nucleotides, are important for cell growth (15,16). Interestingly, the key enzymes in the folate cycle of MTHFD1L not only play an important role in supporting cancer growth but also increase the susceptibility of targeted therapy (10). However, little is known about the specific function of this gene, especially in OSCC. Based on the biosignal analysis, a differential expression of MTHFD1L in OSCC and paracancerous tissues was found. Furthermore, we analyzed the correlation between MTHFD1L expression and survival in OSCC patients and found a powerful connection. Therefore, it is hypothesized that MTHFD1L could play a critical role in the progression of this disease.

We verified the effect of MTHFD1L silencing on cell proliferation, apoptosis and tumorigenesis in OSCC. We found that the value-added rate decreased by 40% and the apoptotic rate decreased by 20% compared with the control group. This finding is also consistent with a previous discovery, which suggests that this gene plays an important regulatory role in the biological behavior of OSCC. In a recent study, these effects were attributed to NADPH reduction and reactive oxygen species (ROS) accumulation. MTHFD1L contributes to the production of NADPH, which is sufficient in combating oxidative stress in OSCC. In addition, it was determined that the expression of MTHFD1L was significantly affected by the mTORC1-4EBP1-eIF4E axis (9). However, the mechanism of shRNA that inhibited *MTHFD1L* gene expression in the cell growth of OSCC is unclear.

In humans, abnormal patterns of protein-protein interactions cause or indicate certain diseased states (17). MTHFD1L directly interacts with the *c-MYC* proto-oncogene and basic helix-loop-helix (bHLH) transcription factor (18). *c-MYC* is located on chromosome 8q24 and belongs to the MYC oncogene family. MYC family proteins regulate various biological responses, including cell proliferation, apoptosis, differentiation and senescence. For example, c-MYC promotes cell proliferation by indirectly activating cyclin E/CDK2 through direct transcriptional activation or the downstream target iron transferrin receptor 1 (TFRC1) (19-21). Furthermore, c-MYC inactivation restored RAS/BRAF-induced senescence, which indicates that continuous MYC signaling is necessary for RAS/BRAF-induced tumorigenesis and tumor progression (21). When combined with the present experimental data, this may indicate that the suppression of MTHFD1L affects c-MYC expression and thereby inhibits tumor cell proliferation and induces apoptosis.

Multiple studies have reported that the regulation of folic acid and its metabolites on cell proliferation and apoptosis are closely related to the p53 pathway in cancer (22,23). Abnormal activation of the p53 pathway may also be involved in the development of OSCC (24). In our study and according to IPA, the p53 pathway might contribute to the abnormal expression of MTHFD1L in OSCC. Therefore, we hypothesized that MTHFD1L may act on OSCC via the p53 pathway. Surprisingly, our data showed that the downregulation of MTHFD1L regulated the activation levels of the p53 signaling pathway. In the molecular regulatory network constructed by IPA analysis, some molecules have changed and several proteins closely related to the p53 pathway have also changed including TP53, GADD45A, FAS and JUN. MTHFD1L directly interacts with the MAGE family member D1 (MAGED) (25,26). MAGED enhances the phosphorylation of the JUN activator protein 1 (AP-1) transcription factor subunit and activates JUN (27). Similar to p53, JUN is also a very unstable protein that is restricted by various ligases and its control of cell cycle progression is dependent on p53 (28). Thus, MTHFD1L knockdown may also affect JUN expression through MAGED and induce cell apoptosis of the tumor. Similarly, proteomic research was used to analyze blood and subcellular fractions from OSCC and the corresponding control samples and found that the c-MYC and p53-related pathways may be involved in the occurrence of OSCC (29).

Conclusions

For the first time, this study revealed a novel MTHFD1L/c-MYC/p53 signaling pathway regulatory network in OSCC. While current data are limited and unable to support an in-depth hypothesis, they provide a direction for future research. Future studies on the role of MTHFD1L in OSCC pathogenesis will facilitate the development of tumor-specific therapeutics that target folate metabolism.

Acknowledgments

Funding: None.

Footnote

Reporting Checklist: The authors have completed the MDAR reporting checklist. Available at http://dx.doi.org/10.21037/tcr-20-2798

Data Sharing Statement: Available at http://dx.doiorg/10.21037/tcr-20-2798

Peer Review File: Available at http://dx.doi.org/10.21037/tcr-20-2798

Conflicts of Interest: All authors have completed the ICMJE uniform disclosure form (available at http://dx.doi.org/10.21037/tcr-20-2798). The authors have no conflicts of interest to declare.

Ethical Statement: The authors are accountable for all aspects of the work in ensuring that questions related to the accuracy or integrity of any part of the work are appropriately investigated and resolved. The study was conducted in accordance with the Declaration of Helsinki (as revised in 2013). The study was approved by ethics board of Beijing Hospital (BJ200768X2). Written informed consent form was obtained from all patients. Experiments were performed under a project license (LA2019103) granted by ethics board of Peking University, in compliance with institutional guidelines for the care and use of animals.

References

1. Zhang SM, Cook NR, Albert CM, et al. Effect of combined folic acid, vitamin B6, and vitamin B12 on cancer risk in women: a randomized trial. JAMA 2008;300:2012-21.
2. Fanidi A, Muller DC, Yuan JM, et al. Circulating Folate, Vitamin B6, and Methionine in Relation to Lung Cancer Risk in the Lung Cancer Cohort Consortium (LC3). J Natl Cancer Inst 2018;110:57-67.
3. Song Y, Manson JE, Lee IM, et al. Effect of combined folic acid, vitamin B(6), and vitamin B(12) on colorectal adenoma. J Natl Cancer Inst 2012;104:1562-75.
4. Kawakita D, Lee YA, Gren LH, et al. The impact of folate intake on the risk of head and neck cancer in the prostate, lung, colorectal, and ovarian cancer screening trial (plco) cohort. Br J Cancer 2018;118:299-306.
5. Sauer J, Mason JB, Choi SW. Too much folate: a risk factor for cancer and cardiovascular disease? Curr Opin Clin Nutr Metab Care 2009;12:30-6.
6. Tedeschi PM, Markert EK, Gounder M, et al. Contribution of serine, folate and glycine metabolism to the ATP, NADPH and purine requirements of cancer cells. Cell Death Dis 2013;4:e877.
7. Momb J, Lewandowski JP, Bryant JD, et al. Deletion of Mthfd1l causes embryonic lethality and neural tube and craniofacial defects in mice. Proc Natl Acad Sci U S A 2013;110:549-54.
8. Pike ST, Rajendra R, Artzt K, et al. Mitochondrial C1-tetrahydrofolate synthase (MTHFD1L) supports the flow of mitochondrial one-carbon units into the methyl cycle in embryos. J Biol Chem 2010;285:4612-20.
9. Li H, Fu X, Yao F, et al. MTHFD1L-Mediated Redox Homeostasis Promotes Tumor Progression in Tongue Squamous Cell Carcinoma. Front Oncol 2019;9:1278.
10. Lee D, Xu IM, Chiu DK, et al. Folate cycle enzyme MTHFD1L confers metabolic advantages in hepatocellular carcinoma. J Clin Invest 2017;127:1856-72.
11. Zhang Y, Xu Y, Li Z, et al. Identification of the key transcription factors in esophageal squamous cell carcinoma. J Thorac Dis 2018;10:148-61.
12. Tanaka T, Ishigamori R. Understanding carcinogenesis for fighting oral cancer. J Oncol 2011;2011:603740.
13. Lee YS, Johnson DE, Grandis JR. An update: emerging drugs to treat squamous cell carcinomas of the head and neck. Expert Opin Emerg Drugs 2018;23:283-99.
14. Gebregiworgis T, Purohit V, Shukla SK, et al. Glucose Limitation Alters Glutamine Metabolism in MUC1-Overexpressing Pancreatic Cancer Cells. J Proteome Res 2017;16:3536-46.
15. Burgos-Barragan G, Wit N, Meiser J, et al. Mammals divert endogenous genotoxic formaldehyde into one-carbon metabolism. Nature 2017;548:549-54.
16. Zhang J, Pavlova NN, Thompson CB. Cancer cell metabolism: the essential role of the nonessential amino acid, glutamine. EMBO J 2017;36:1302-15..
17. Kuzmanov U, Emili A. Protein-protein interaction

networks: probing disease mechanisms using model systems. Genome Med 2013;5:37.
18. Hue M, Riffle M, Vert JP, et al. Large-scale prediction of protein-protein interactions from structures. BMC Bioinformatics 2010;11:144.
19. Hung CL, Wang LY, Yu YL, et al. A long noncoding RNA connects c-Myc to tumor metabolism. Proc Natl Acad Sci U S A 2014;111:18697-702.
20. Beaulieu ME, Castillo F, Soucek L. Structural and Biophysical Insights into the Function of the Intrinsically Disordered Myc Oncoprotein. Cells 2020;9:1038.
21. Watt FM, Frye M, Benitah SA. MYC in mammalian epidermis: how can an oncogene stimulate differentiation? Nat Rev Cancer 2008;8:234-42.
22. Kuo CT, Chang C, Lee WS. Folic acid inhibits COLO-205 colon cancer cell proliferation through activating the FRα/c-SRC/ERK1/2/NFκB/TP53 pathway: in vitro and in vivo studies. Sci Rep 2015;5:11187.
23. Wang Z, Xing W, Song Y, et al. Folic Acid Has a Protective Effect on Retinal Vascular Endothelial Cells against High Glucose. Molecules 2018;23:2326.
24. Wang X, Bai Y, Han Y, et al. Downregulation of GBAS regulates oral squamous cell carcinoma proliferation and apoptosis via the p53 signaling pathway. Onco Targets Ther 2019;12:3729-42.
25. Zhang F, Zakaria SM, Högqvist Tabor V, et al. MYC and RAS are unable to cooperate in overcoming cellular senescence and apoptosis in normal human fibroblasts. Cell Cycle 2018;17:2697-715.
26. Krishna A, Bhatt MLB, Singh V, et al. Differential Expression of c-fos Proto-Oncogene in Normal Oral Mucosa versus Squamous Cell Carcinoma. Asian Pac J Cancer Prev 2018;19:867-74.
27. Cao SS, Kaufman RJ. Endoplasmic reticulum stress and oxidative stress in cell fate decision and human disease. Antioxid Redox Signal 2014;21:396-413.
28. Schreiber M, Kolbus A, Piu F, et al. Control of cell cycle progression by c-Jun is p53 dependent. Genes Dev 1999;13:607-19.
29. Wang Z, Feng X, Liu X, et al. Involvement of potential pathways in malignant transformation from oral leukoplakia to oral squamous cell carcinoma revealed by proteomic analysis. BMC Genomics 2009;10:383.

Cite this article as: Zhao L, Cheng Z, Lu Z, Jin J. NAD-dependent methylenetetrahydrofolate dehydrogenase inhibits oral squamous cell carcinoma cell proliferation and promotes apoptosis. Transl Cancer Res 2021;10(3):1457-1469. doi: 10.21037/tcr-20-2798

